Table of content

1. Reaction of C2, C6, C7 and C8 with AcOH (UV-vis spectroscopy)

(a)

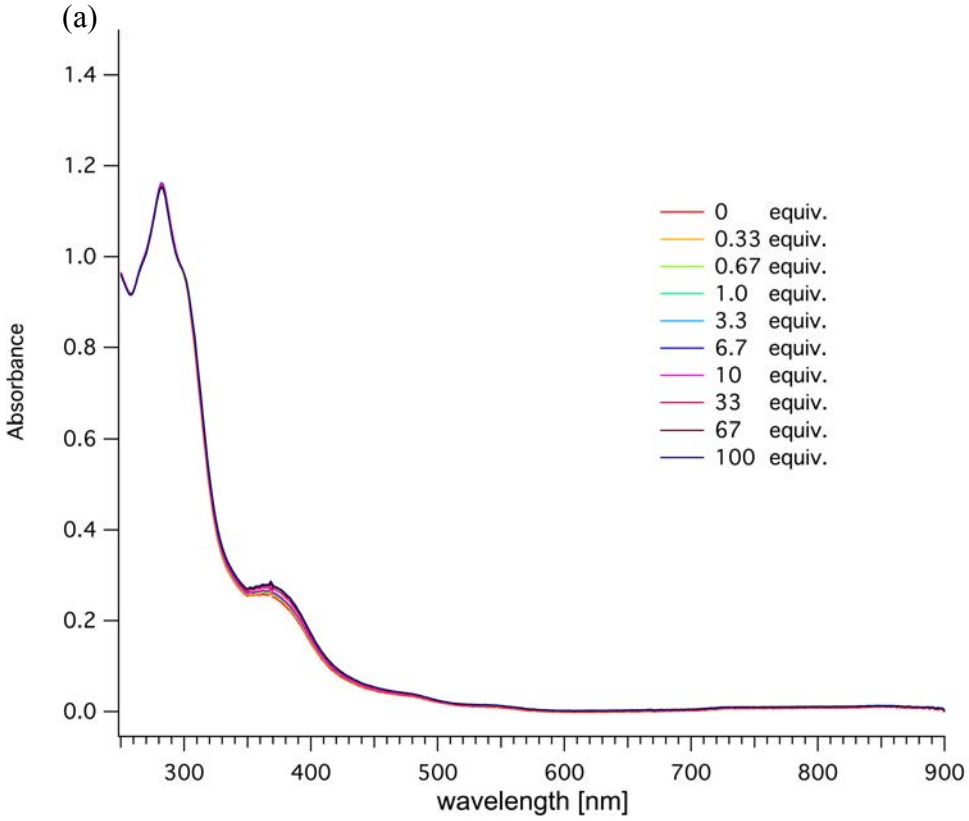

(b)

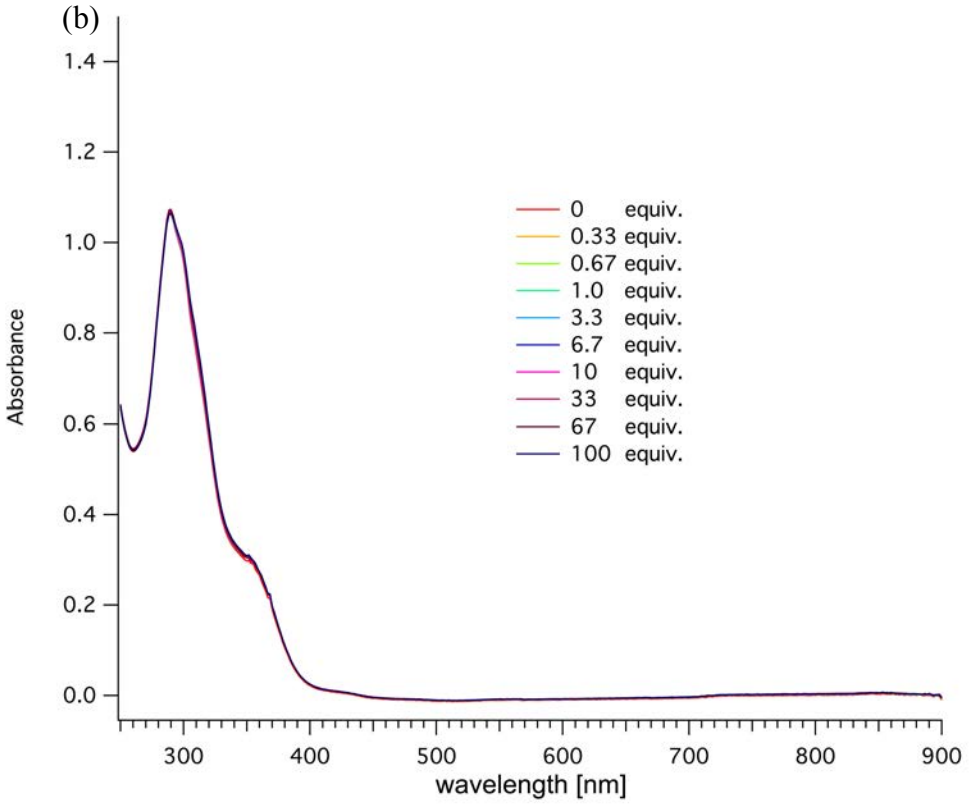

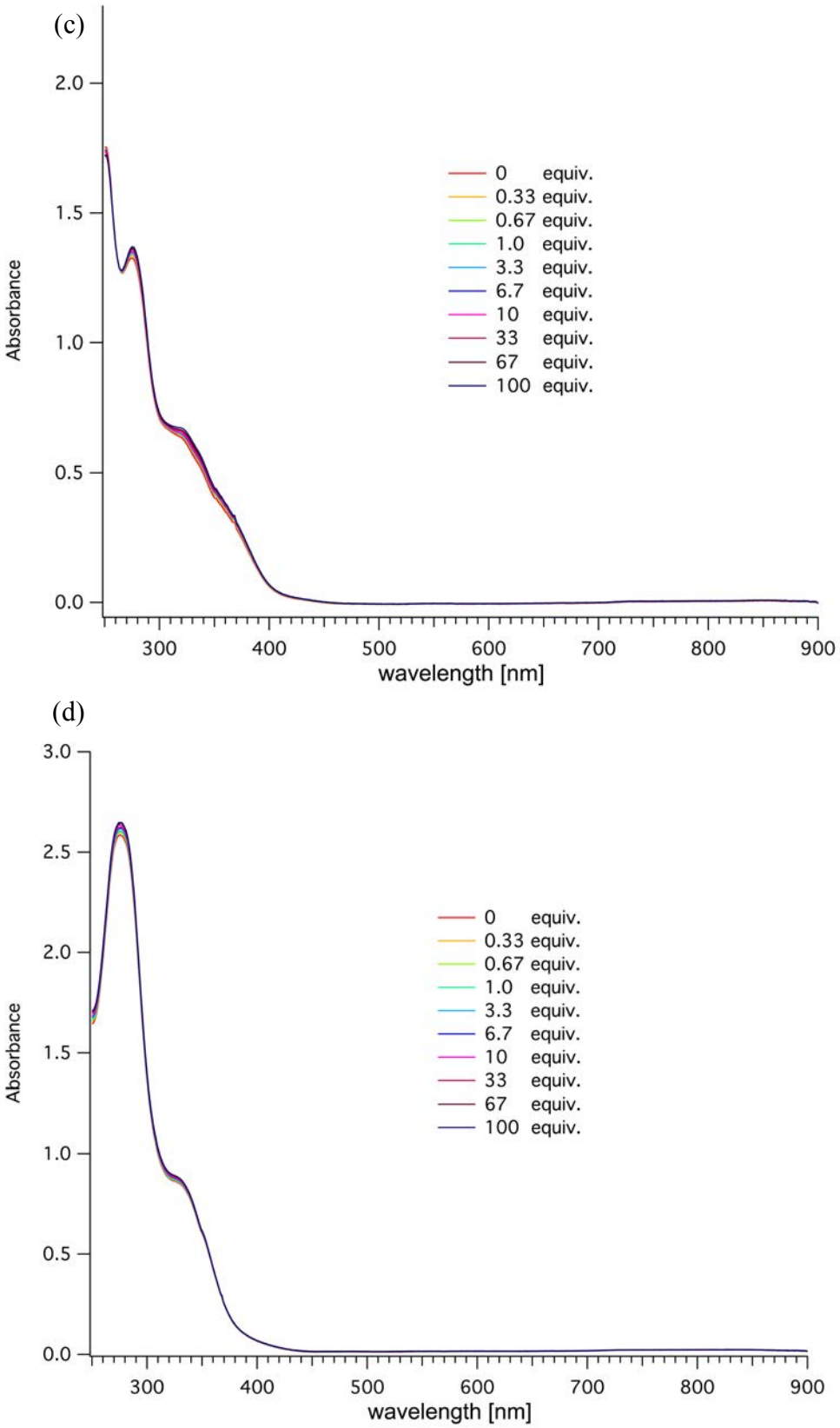

Fig. S1 UV-vis spectrum of the complex (a) **C2**, (b) **C6**, (c) **C7**, (d) **C8**, at 25 μM before and after addition of increasing equivalents of acetic acid (0.33 – 100 equiv.)

2. Cyclic voltammetry in presence of acids

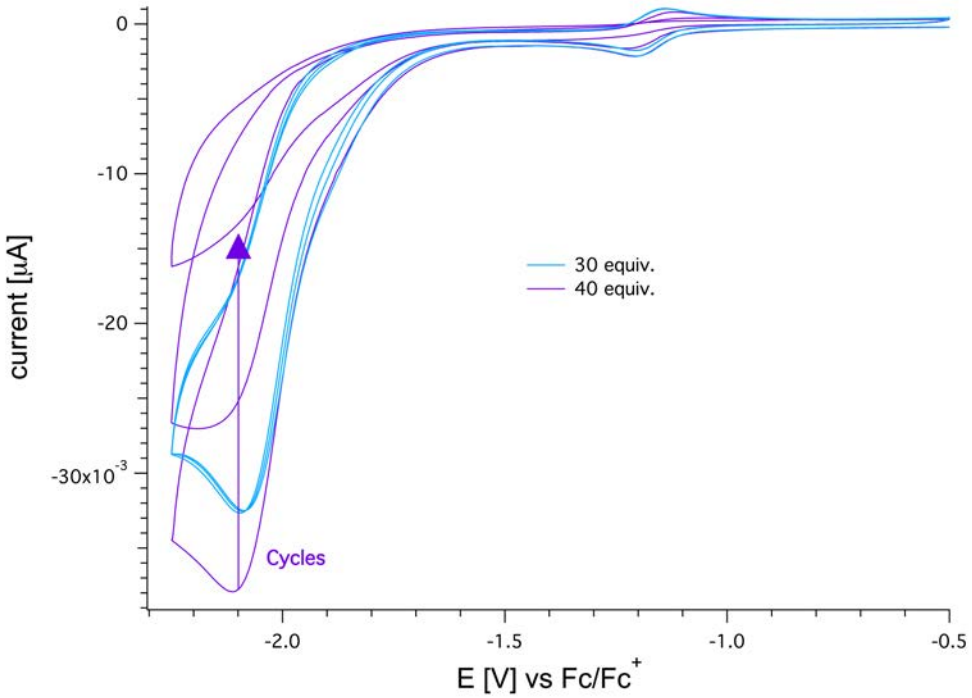

Fig. S2 Cyclic voltammograms (50 mV/sec, three cycles) for complex **C1** (1.0 mM) in CH_3CN in the presence of acetic acid (30 and 40 equiv.). **C1** decomposes in the presence of 40 equiv. of acid.

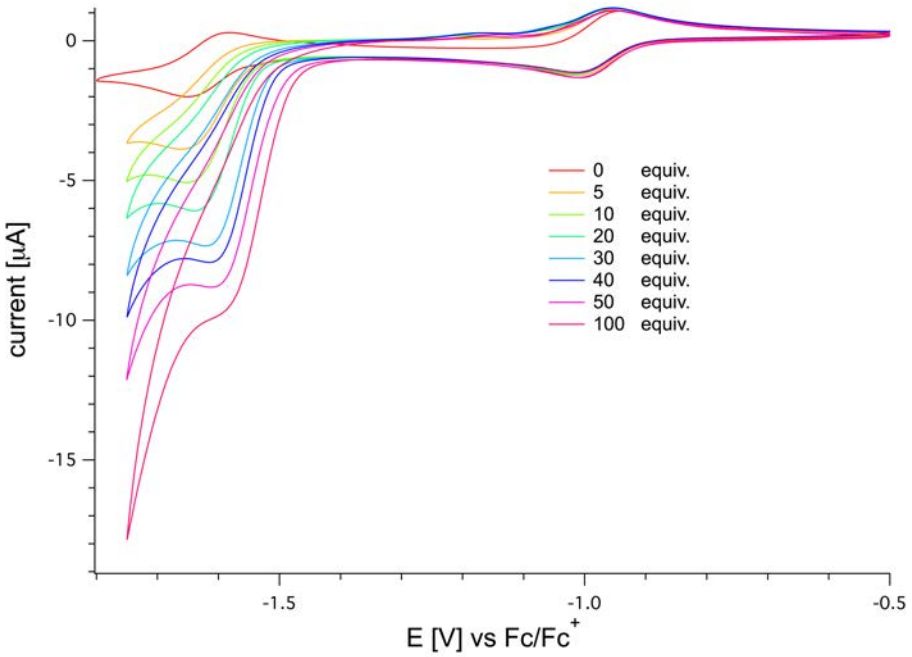

Fig. S3 Cyclic voltammograms (50 mV/sec, second scan) for complex **C3** (1.0 mM) in CH_3CN in the presence of increasing equivalents of acetic acid (0 – 100 equiv.).

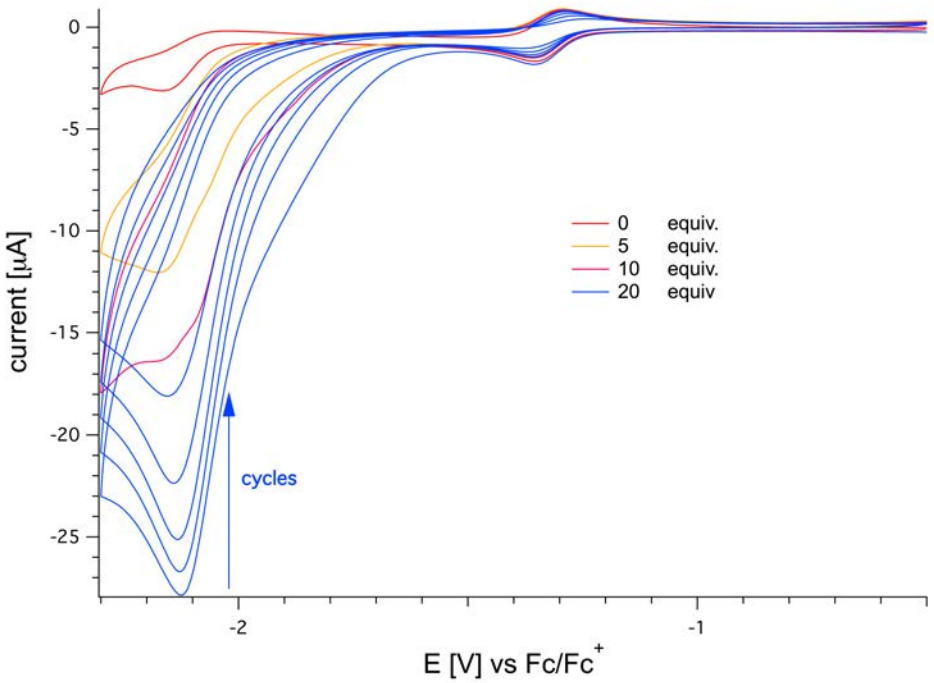

Fig. S4 Cyclic voltammograms (50 mV/sec, second cycle) for complex **C4** (1.0 mM) in CH_3CN in the presence of increasing equivalents of acetic acid (0 – 20 equiv.). At 20 equiv. of acetic acid, cycles do not overlay. **C4** decomposes in the presence of 20 equiv. of acid.

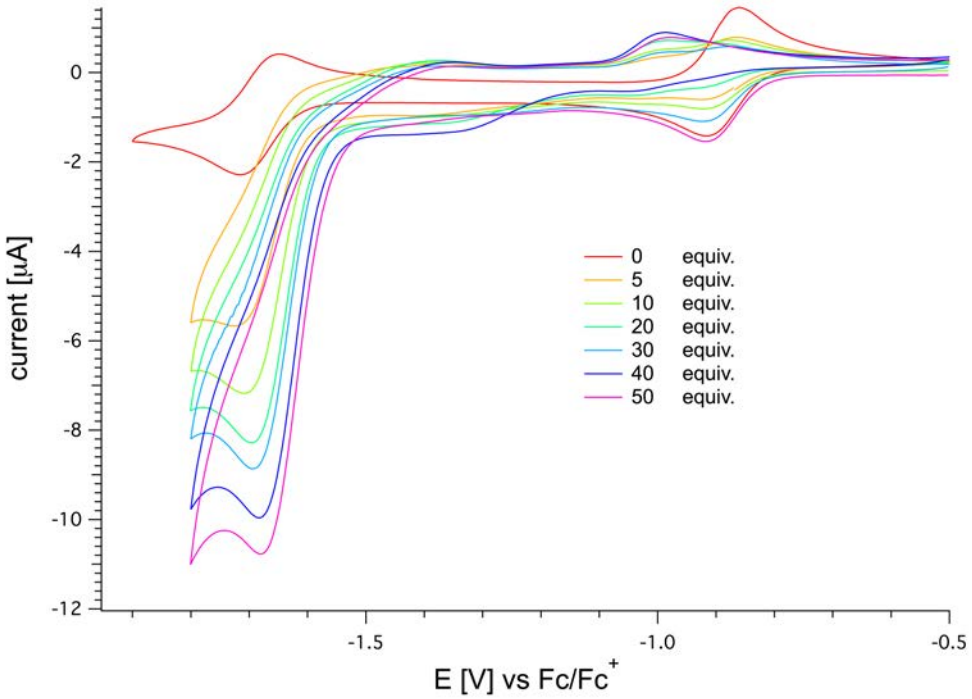

Fig. S5 Cyclic voltammograms (50 mV/sec, second cycle) for complex **C5** (1.0 mM) in CH_3CN in the presence of increasing equivalents of acetic acid (0 – 50 equiv.). **C5** starts decomposing in the presence of 5 equiv. of acid.

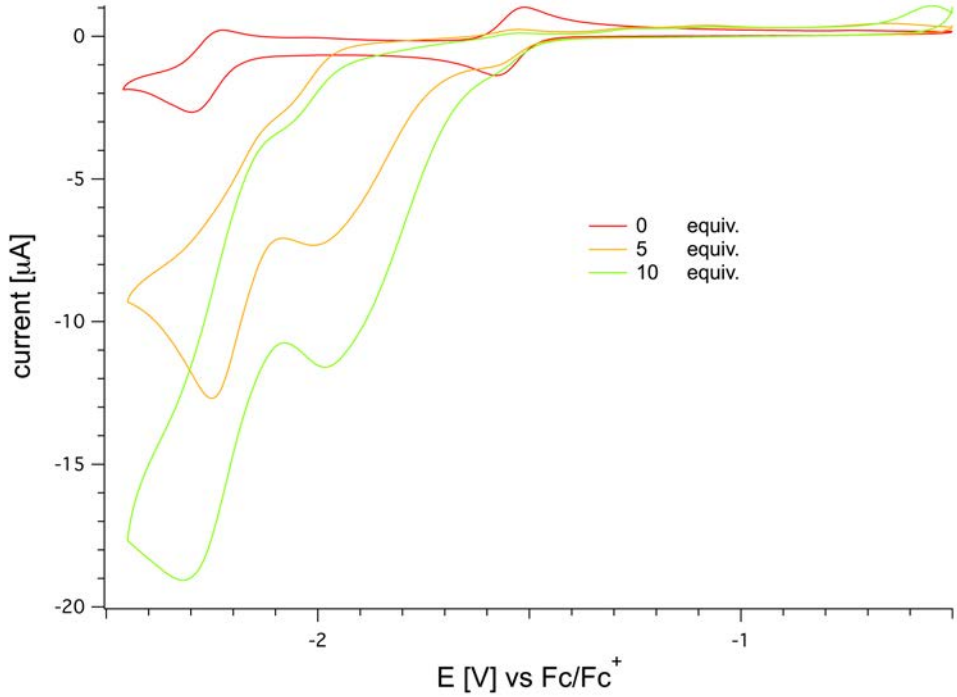

Fig. S6 Cyclic voltammograms (50 mV/sec, second cycle) for complex **C6** (1.0 mM) in CH_3CN in the presence of increasing equivalents of acetic acid (0 – 10 equiv.). **C6** starts decomposing in the presence of 5 equiv. of acid.

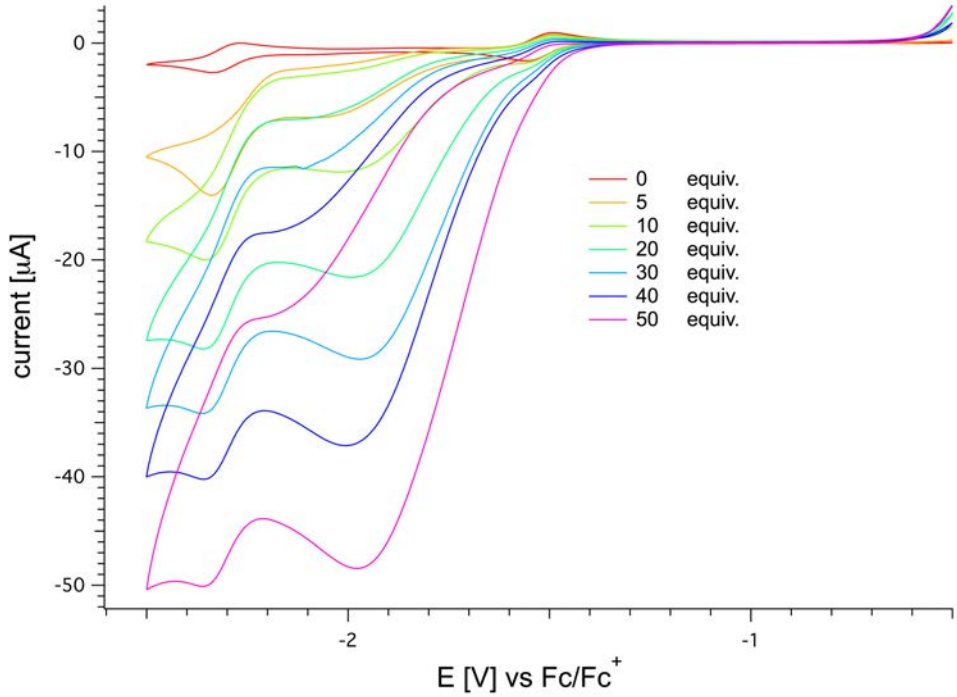

Fig. S7 Cyclic voltammograms (50 mV/sec, second cycle) for complex **C7** (1.0 mM) in CH_3CN in the presence of increasing equivalents of acetic acid (0 – 50 equiv.).

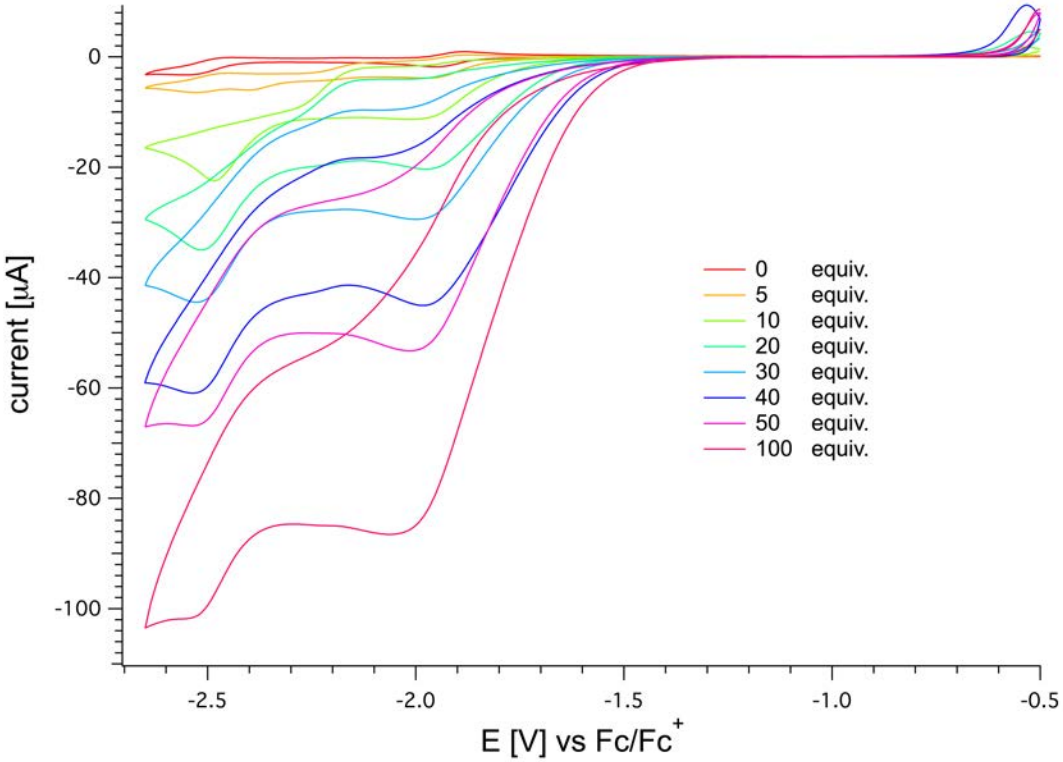

Fig. S8 Cyclic voltammograms (50 mV/sec, second cycle) for complex **C8** (1.0 mM) in CH_3CN in the presence of increasing equivalents of acetic acid (0 – 100 equiv.).

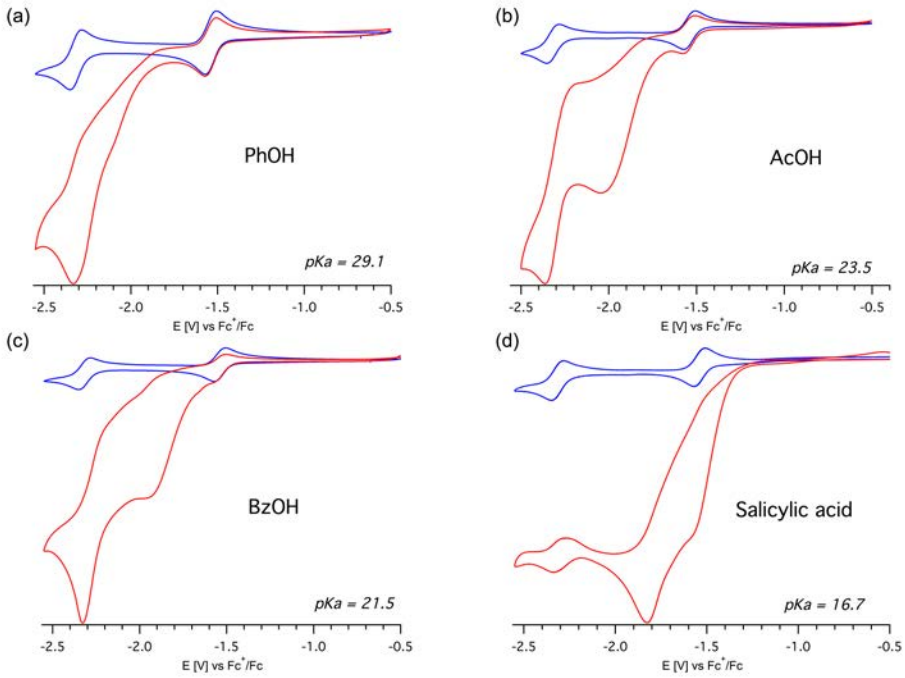

Fig. S9 Cyclic voltammograms for the complexes **C7** (1.0 mM, in blue) in CH_3CN (50 mV/s, 0.1 TBAP), and in the presence of 10 mM of (a) acetic acid, (b) benzoic acid, (c) salicylic acid.

3. Determination of turnover frequency (TOF)

We used the standard i_c/i_p analysis, even though this gives an underestimated value. For that purpose, we have checked that the reaction was first order with respect to concentration of catalyst and second order with respect to concentration of acetic acid. Taking into account that i_c is independent on scan rate (larger than 0.25 V s^{-1}) and after verification that i_p varies linearly as a function of $\nu^{1/2}$ (**Fig. S10 - Fig. S13**), the reaction rate can be estimated using the following equation:

$$\frac{i_c}{i_p} = \frac{n}{0.4463}\sqrt{\frac{RTk}{F\nu}}\,[H^+]$$

and

$$TOF = k\,x\,[H^+]^2 \quad (TOF = 10^{-2}\,k, \text{ for } [H^+] = 0.1\ M)$$

where i_c is the maximal peak current in the presence of acid, i_p is the peak current in the absence of acid, n is the number of electrons (in eq. mol^{-1}), R is the gas constant (8.31 V C mol^{-1} K^{-1}), T is the temperature (in K), F is Faraday's constant (96485 C eq. mol^{-1}), ν is the scan rate (in V s^{-1}), k is the rate constant for the electrocatalytic HER (in M^{-2} s^{-1}), and $[H]^+$ is the concentration of acetic acid (in M). For complex **C1**, **C2** and **C8**, TOF values were obtained after experiments carried out at different scan rate values in the presence of increasing concentration of acetic acid (Fig. S15, Fig. S18, Fig. S22). From these data, the slope of the plot $i_c/i_p = f([H^+])$ (Fig. S16, Fig. S19, Fig. S23) allows calculating the k and TOF values.

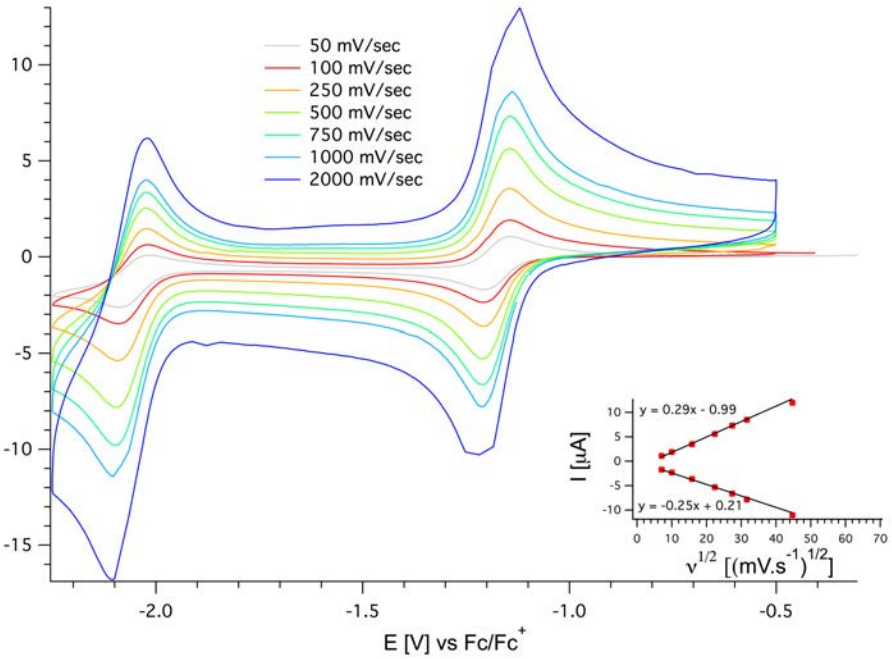

Fig. S10 Cyclic voltammograms of the complex **C1** (1.0 mM) in CH_3CN (0.1 M TBAP) at increasing scan rates (from 50 to 2000 mV/sec). Inset: plot of the Co^{2+}/Co^{+} anodic and cathodic peak intensity current versus $\nu^{1/2}$.

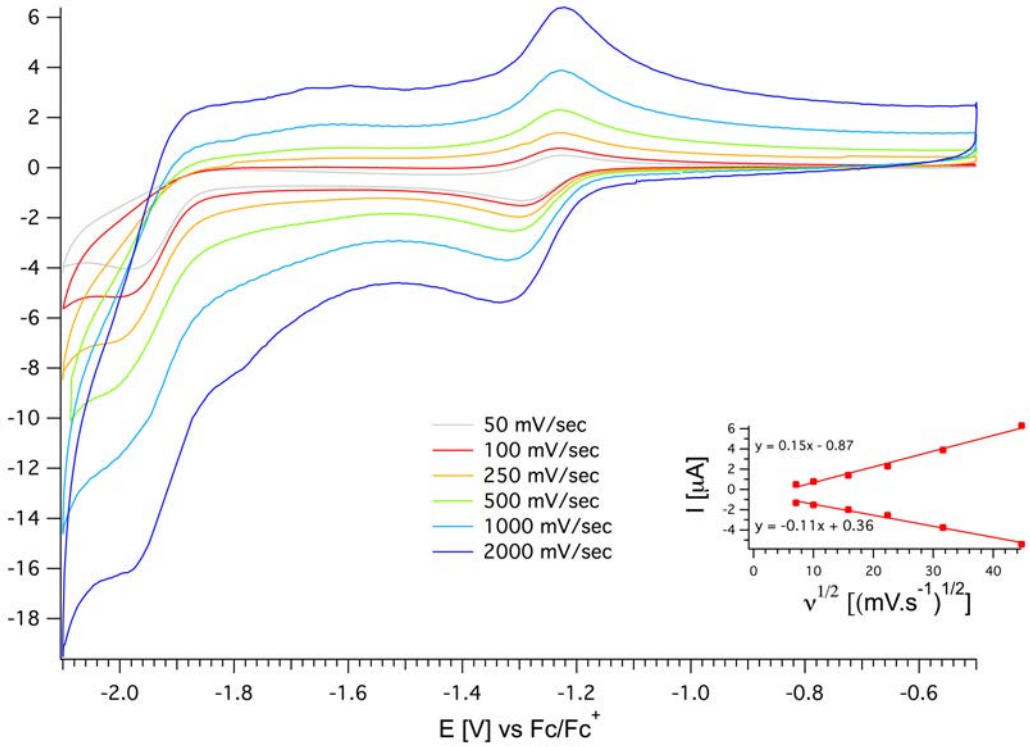

Fig. S11 Cyclic voltammograms of the complex **C2** (1.0 mM) in CH_3CN (0.1 M TBAP) at increasing scan rates (from 50 to 2000 mV/sec). Inset: plot of the Co^{2+}/Co^{+} anodic and cathodic peak intensity current versus $\nu^{1/2}$.

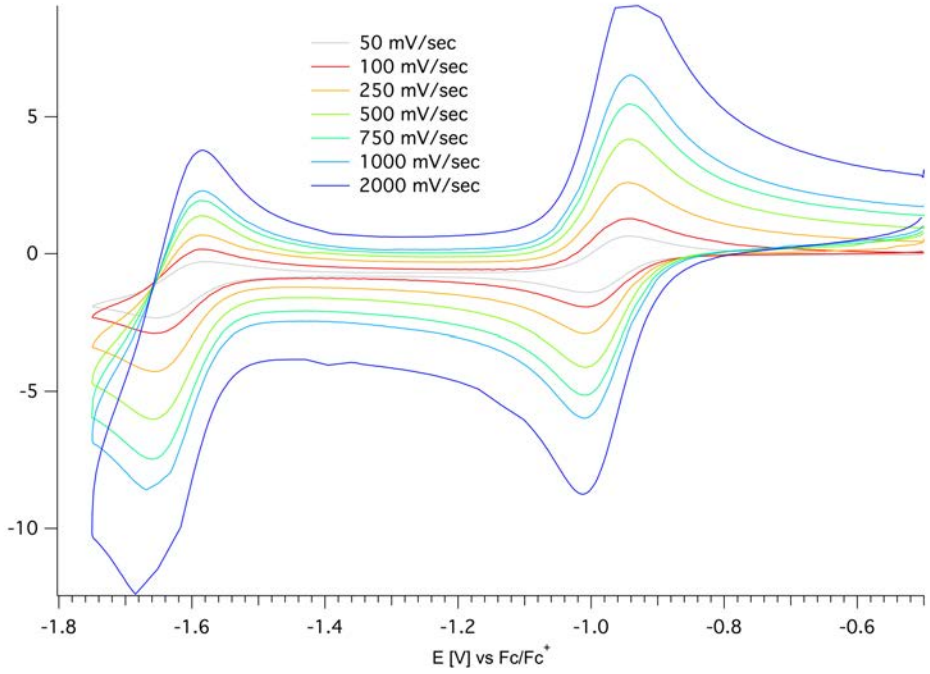

Fig. S12 Cyclic voltammograms of the complex **C3** (1.0 mM) in CH_3CN (0.1 M TBAP) at increasing scan rates (from 50 to 2000 mV/sec). Inset: plot of the Co^{2+}/Co^{+} anodic and cathodic peak intensity current versus $\nu^{1/2}$.

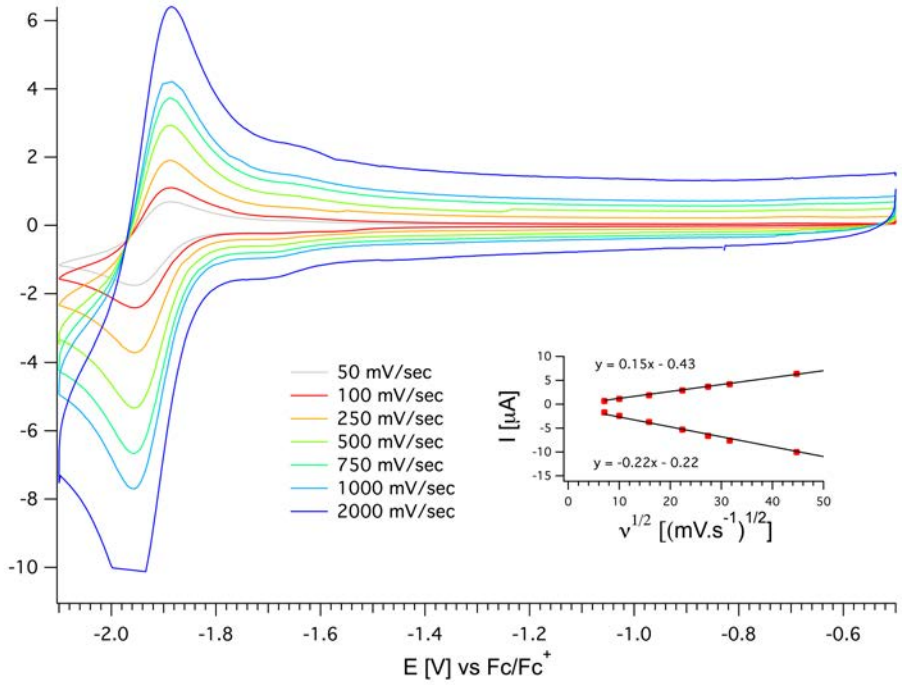

Fig. S13 Cyclic voltammograms of the complex **C8** (1.0 mM) in CH_3CN (0.1 M TBAP) at increasing scan rates (from 50 to 2000 mV/sec). Inset: plot of the Co^{2+}/Co^{+} anodic and cathodic peak intensity current versus $\nu^{1/2}$.

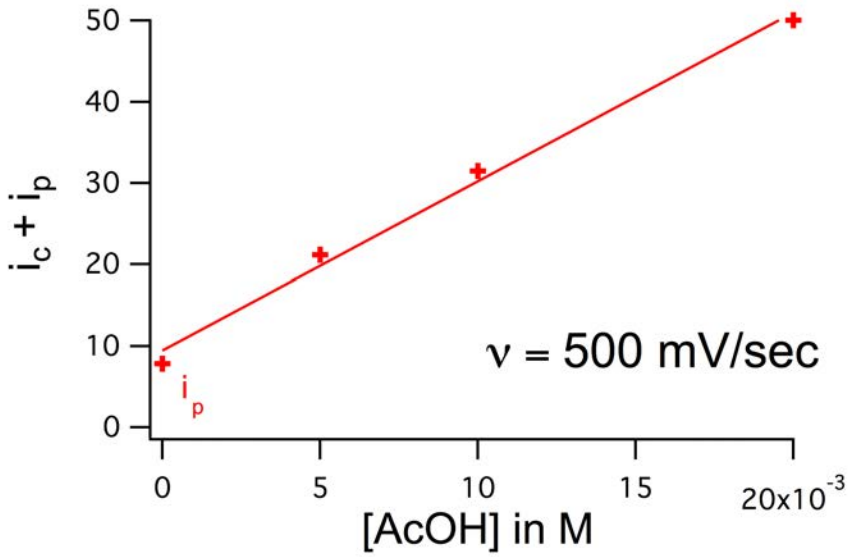

Fig. S14 Dependence of the catalytic current intensity with respect to the concentration of acetic acid (500 mV/sec) in the case of **C1** at -2.04 V.

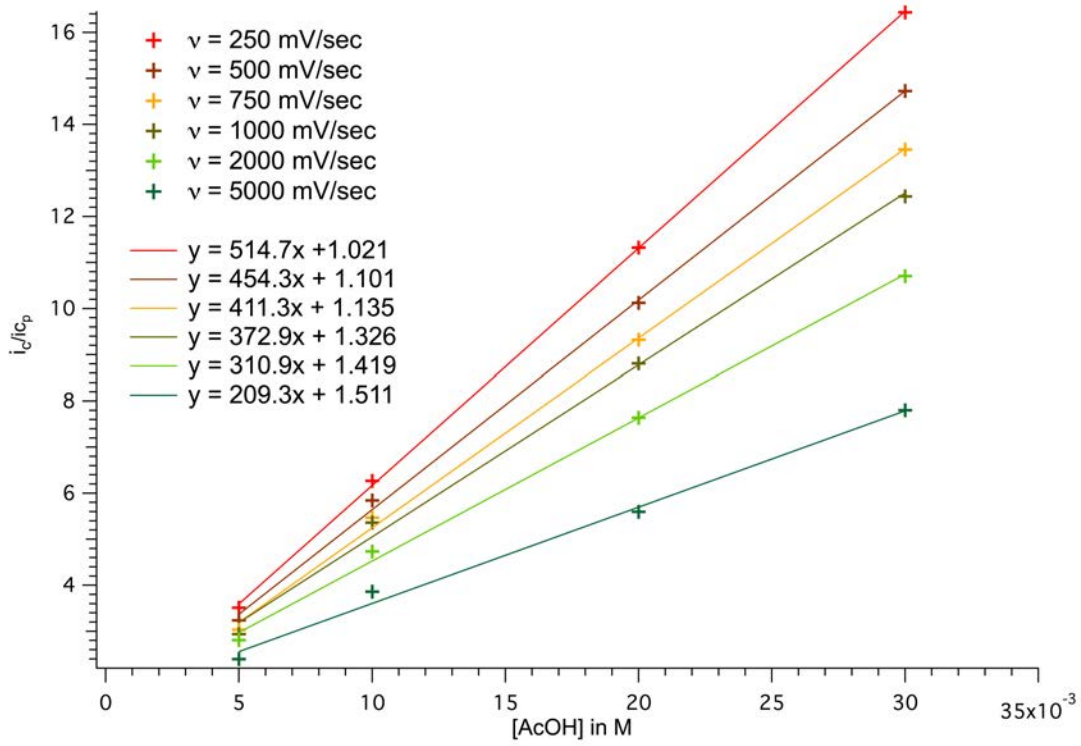

Fig. S15 Plot of i_c/i_p values as a function of acetic acid concentration for 1.0 mM of complex **C1** in 0.1 M TBAP in acetonitrile at a glassy carbon electrode.

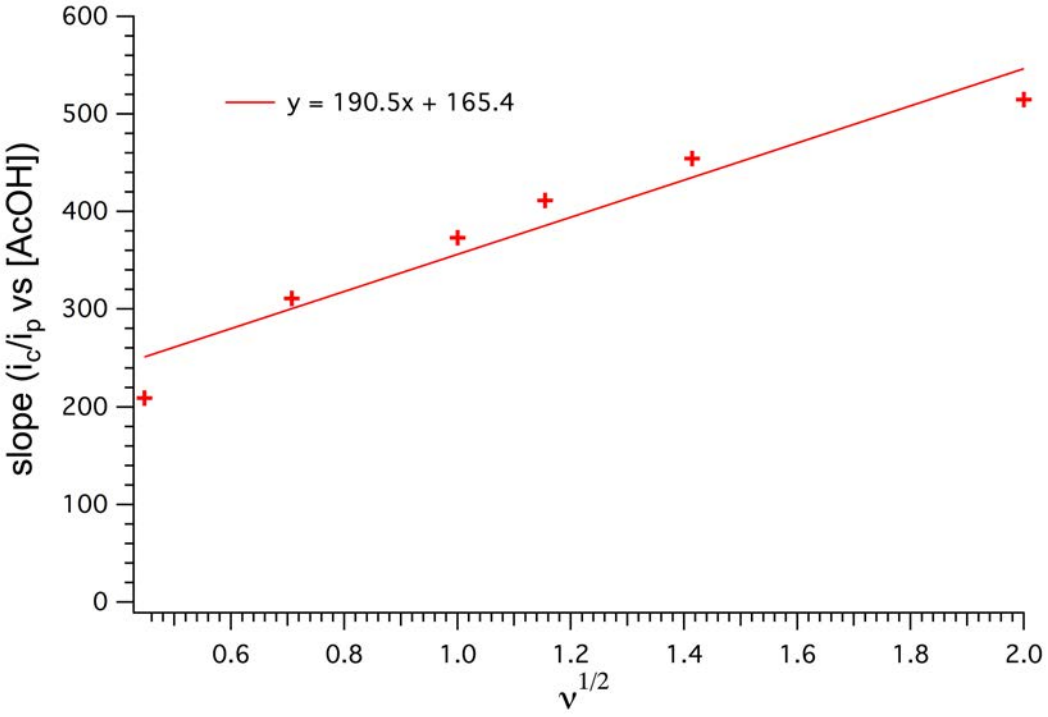

Fig. S16 Plot of the slopes from Fig. S15 vs $\nu^{1/2}$ for complex **C1**.

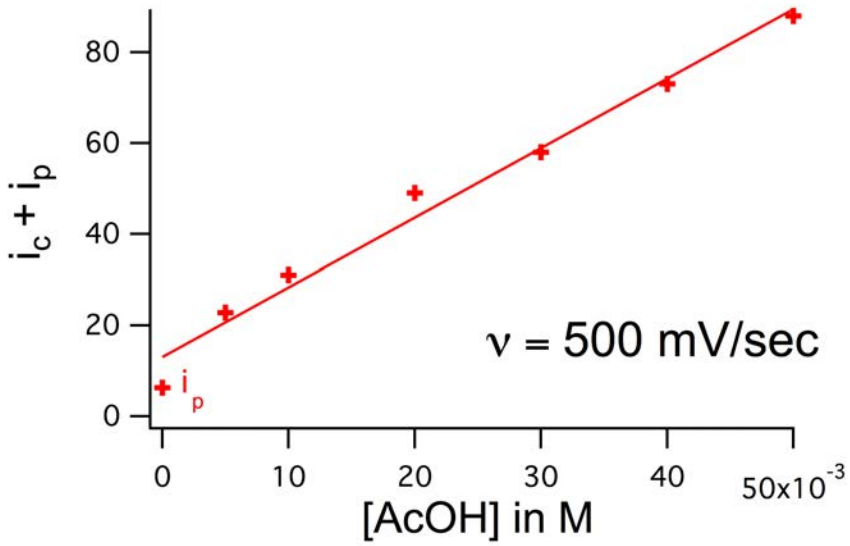

Fig. S17 Linear dependence of the catalytic current intensity with respect to the concentration of acetic acid (500 mV/sec) in the case of **C2** at -1.91 V.

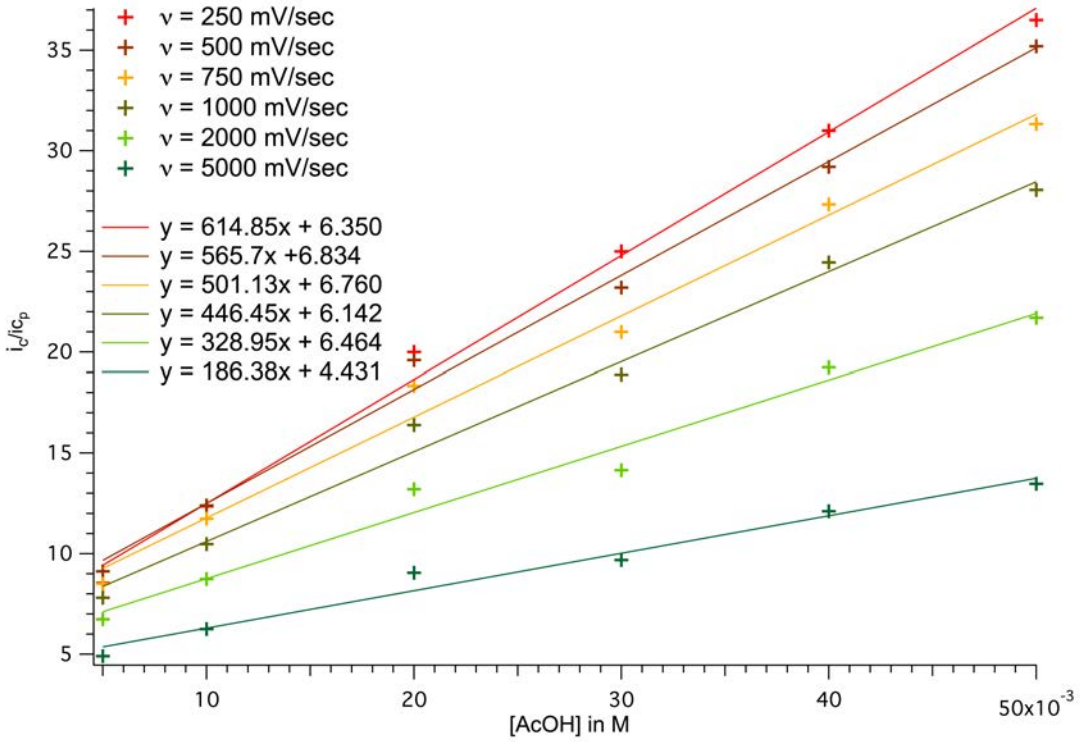

Fig. S18 Plot of i_c/i_p values as a function of acetic acid concentration for 1.0 mM of complex **C2** in 0.1 M TBAP in acetonitrile at a glassy carbon electrode.

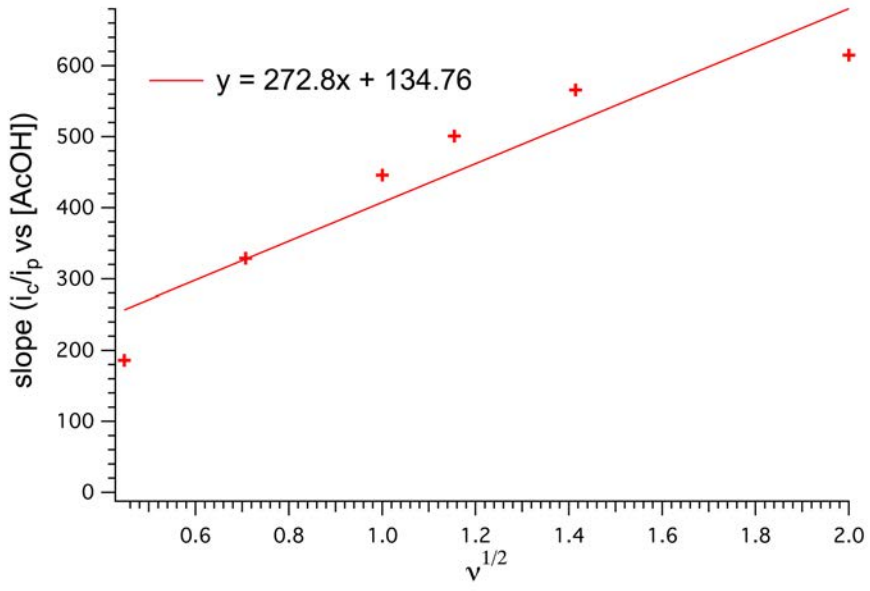

Fig. S19 Plot of the slopes from Fig. S17 vs $\nu^{1/2}$ for complex **C2**.

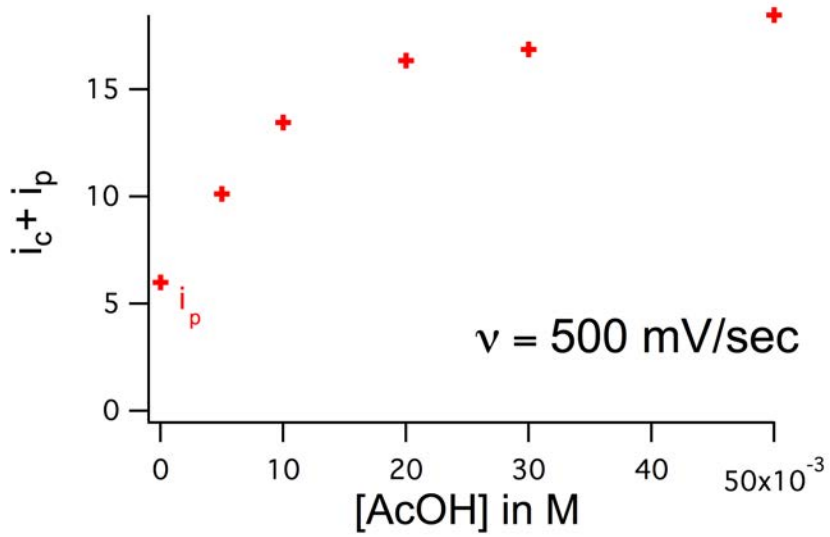

Fig. S20 Dependence of the catalytic current intensity with respect to the concentration of acetic acid (500 mV/sec) in the case of **C3** at -1.61 V.

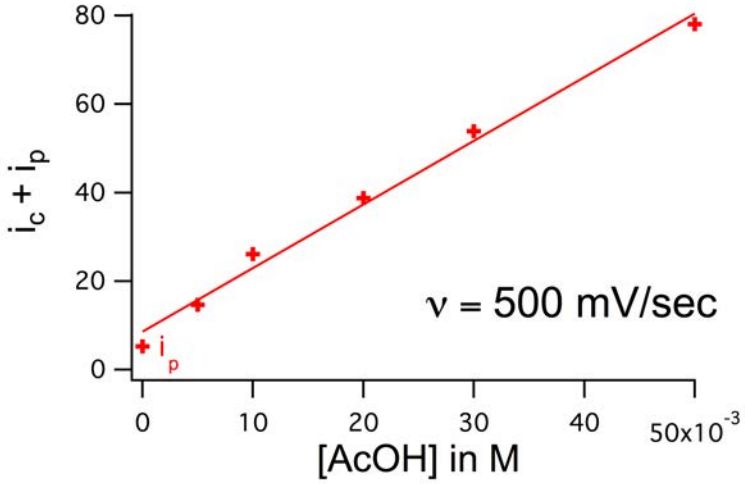

Fig. S21 Linear dependence of the catalytic current intensity with respect to the concentration of acetic acid (500 mV/sec) in the case of **C8** at -1.92 V.

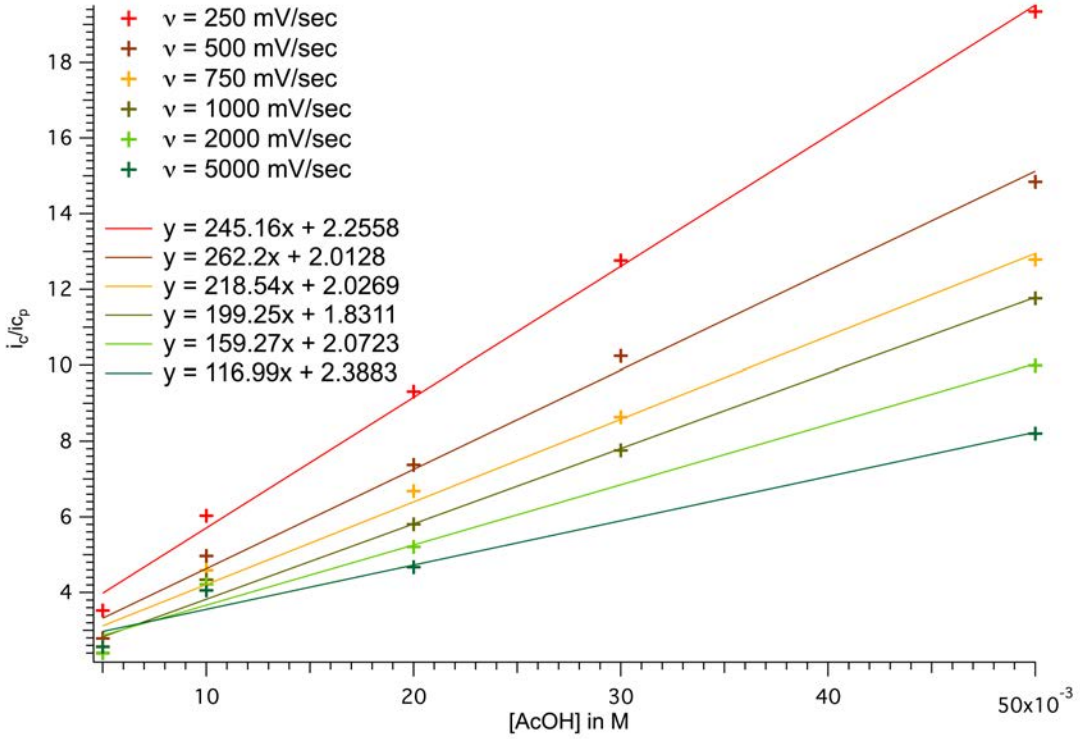

Fig. S22 Plot of i_c/i_p values as a function of acetic acid concentration for 1.0 mM of complex **C8** in 0.1 M TBAP in acetonitrile at a glassy carbon electrode.

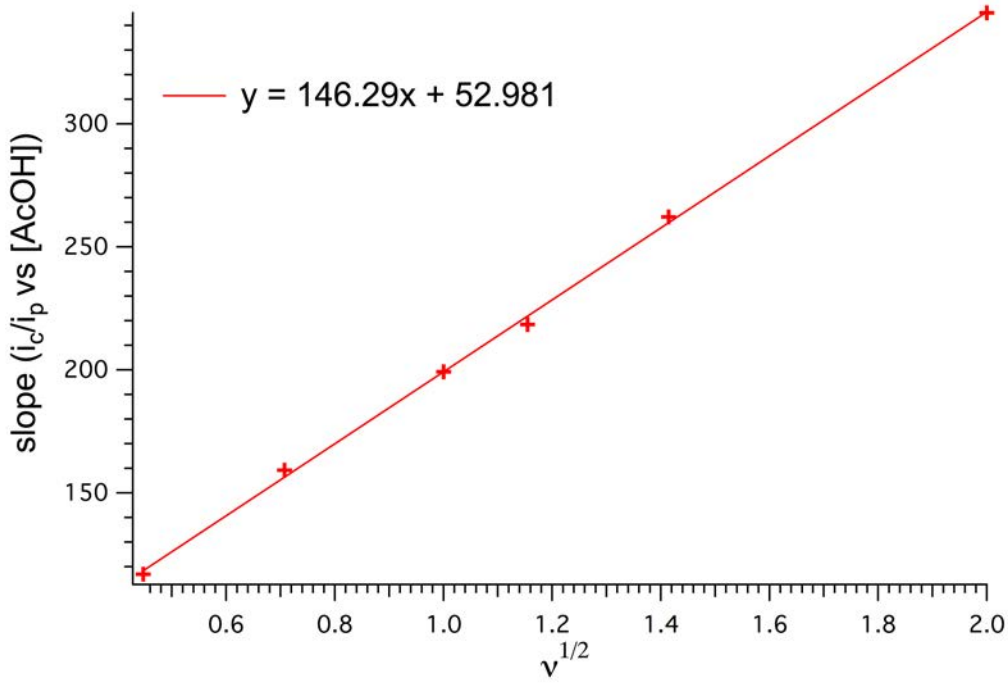

Fig. S23 Plot of the slopes from Fig. S22 vs $\nu^{1/2}$ for complex **C8**.

4. Controlled-potential electrolysis

Electrolysis experiments were carried out at room temperature in a custom-built, gas-tight two compartments electrochemical cell specific for mercury. The electrochemical cell contains two compartments, a cathodic compartment with a mercury pool as a working electrode (1.5 cm diameter, 0.6 mL mercury); a reference electrode made of silver wire coated with silver chloride in saturated KCl aqueous solution isolated from the working solution by a vycor frit. The anodic compartment contains a platinum wire of 0.5 mm diameter separated from the cathodic compartment with a glass frit of fine porosity.

The working compartment was filled with an acetonitrile solution with 0.1 M TBAP, containing 1.0 mM of catalyst and 0.1 M acetic acid. The counter compartment was filled with an acetonitrile solution with 0.1 M TBAP. They were purged with N_2 gas for 30 min before electrolysis and were constantly stirred.

H_2 measurements were performed by gas chromatography using a Shimadzu GC-2014 chromatograph equipped with a Quadrex column for gas separation, a thermal conductivity detector (TCD) for analyte quantification, and using N_2 as a carrier gas. Gas chromatography calibration curves were made by sampling known volumes of pure H_2 gas in diluted N_2.

Faradic yields were calculated by measuring H_2 produced in the headspace gas (50 mL) removed as aliquots with a gas-tight syringe by GC. The typical volume of gas injected was 50 μL.

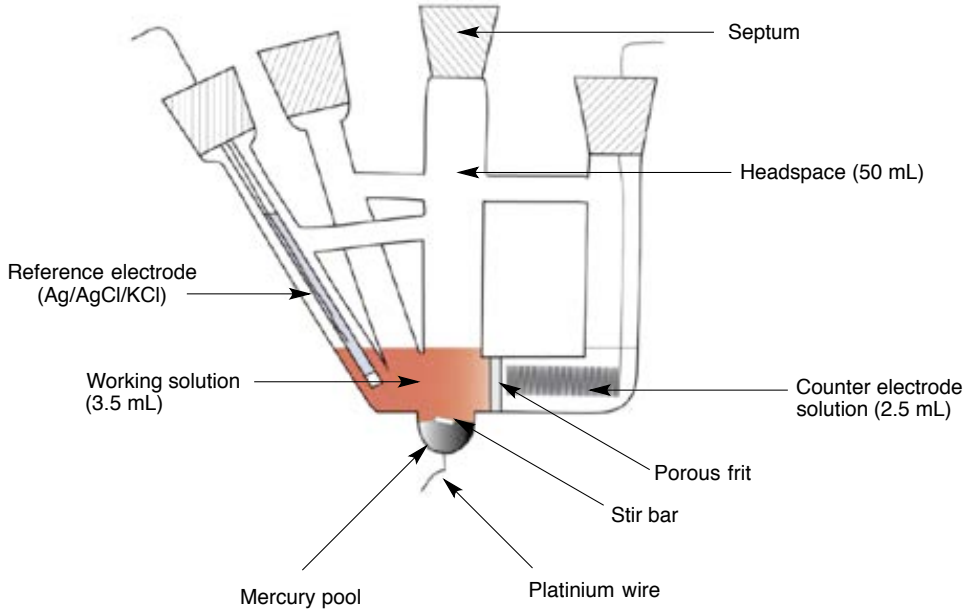

Fig. S24 Representation of the electrochemical cell used for an electrolysis experiment.

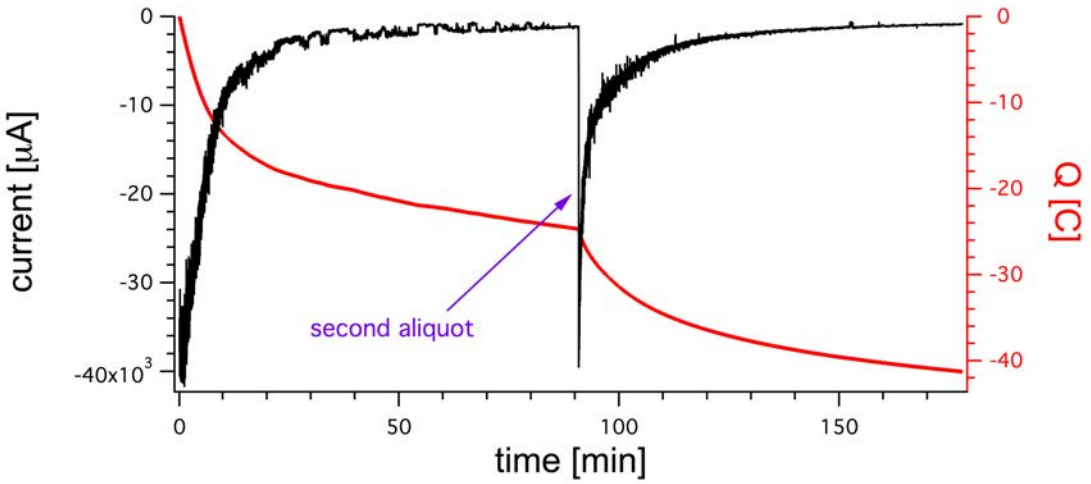

Fig. S25 CPE current of **C2** at -1.91 V and after addition of an aliquot of 100 equiv. of acetic acid.

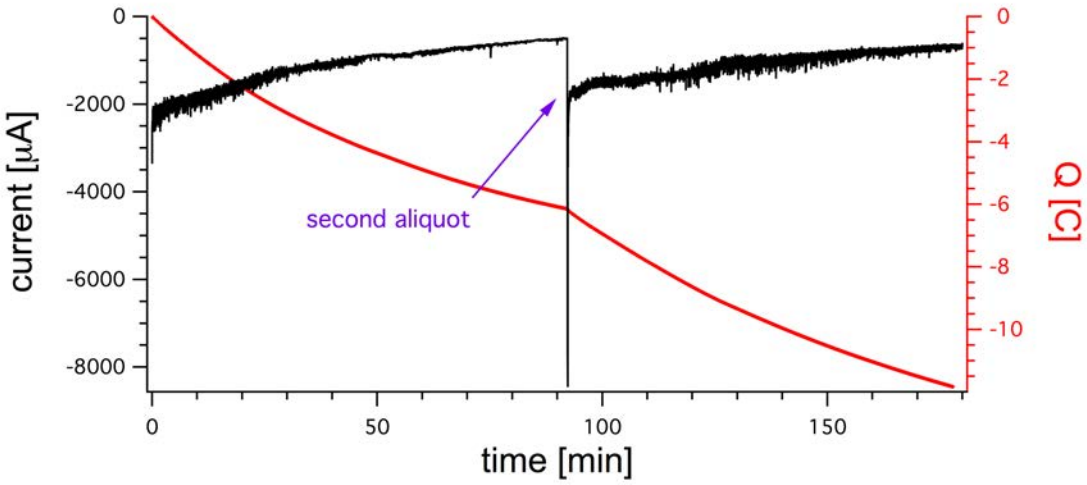

Fig. S26 CPE current of **C3** at -1.65 V and after addition of an aliquot of 100 equiv. of acetic acid.

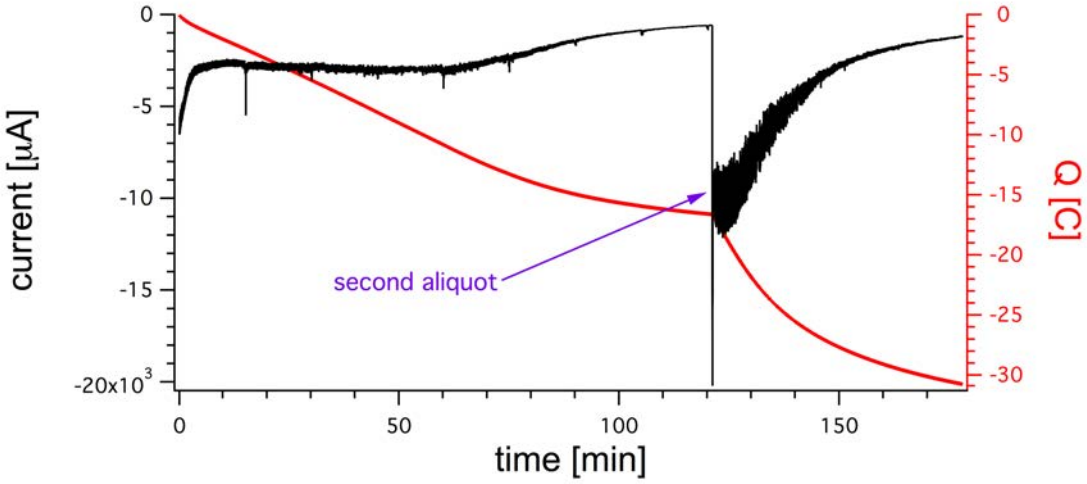

Fig. S27 CPE current of **C8** at -1.91 V and after addition of an aliquot of 100 equiv. of acetic acid.

5. DFT calculations

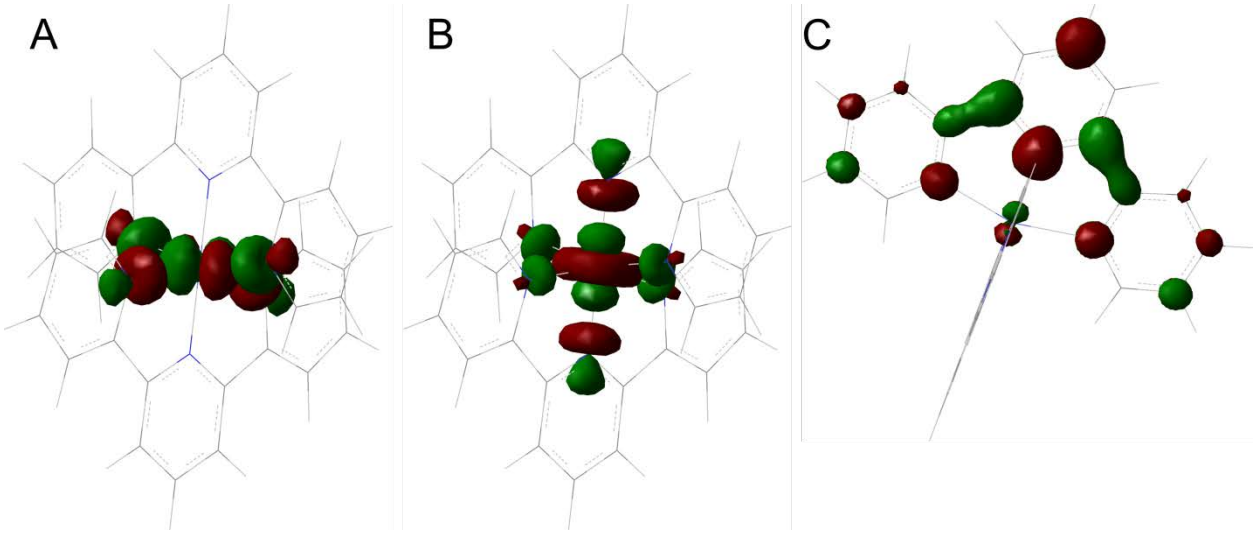

Fig. S28 Calculated (M06-L/6-311+G(d,p) level in CH_3CN, isovalue = 0.05) SOMOs of (A) $\mathbf{C1}^{|2+|}$ in its doublet state, (B) $\mathbf{C1}^{|+|}$ (triplet ground state) showing that the second electron is localized on the σ* Co $3dz^2$ orbital, and (C) **C1** in its quartet state, showing the third electron delocalized on the tpy ligand.

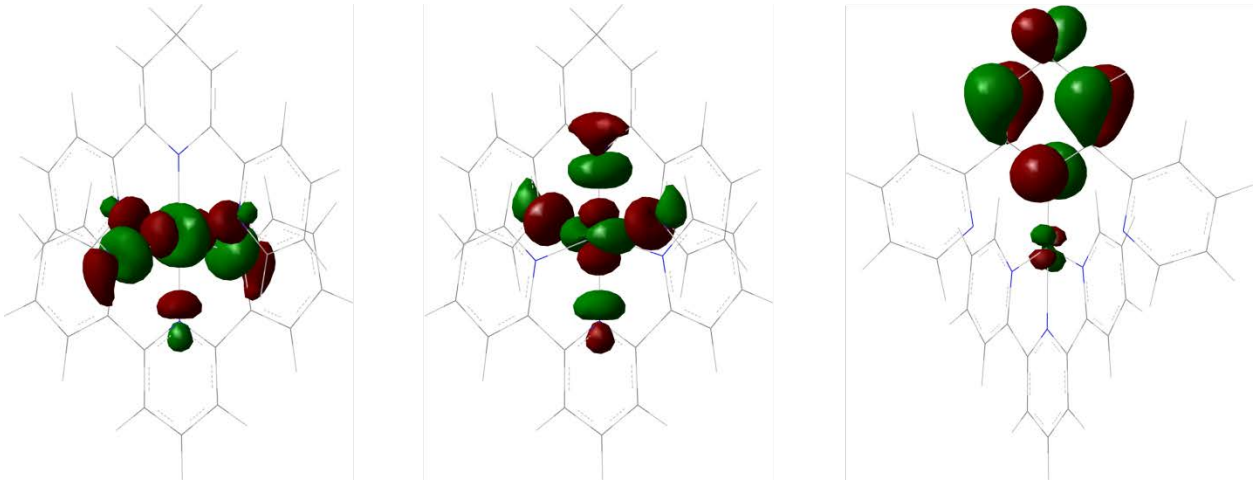

Fig. S29 SOMOs of $\mathbf{(C1\text{-}CH)}^{|+|}$ in its quartet ground state (isovalue = 0.05) showing the electron density localization on the σ* Co $3dx^2\text{-}y^2$ orbital, σ* Co $3dz^2$ orbital, and on the protonated central pyridyl ring, respectively.

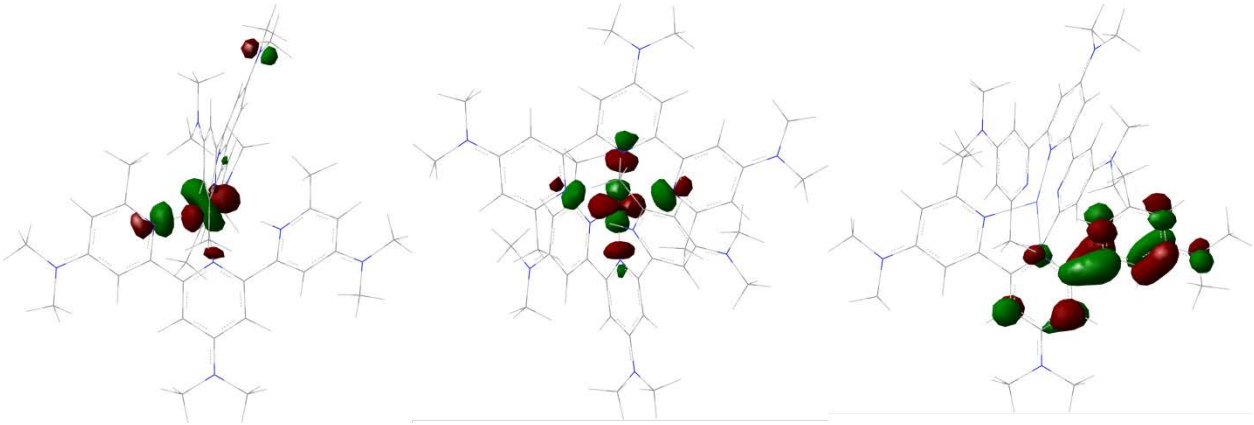

Fig. S30 SOMOs of (**C8-NH**)$^{[+]}$ in its quartet ground state (isovalue = 0.05), showing the electron density localization on the σ* Co $3dx^2$-y^2 orbital, σ* Co $3dz^2$ orbital, and on the protonated distal pyridyl ring, respectively.